Domain structure and phase transition in Sc-doped zirconia

2002 J. Phys.: Condens. Matter 14 135

(http://iopscience.iop.org/0953-8984/14/2/301)

INSTITUTE OF PHYSICS PUBLISHING JOURNAL OF PHYSICS: CONDENSED MATTER

J. Phys.: Condens. Matter **14** (2002) 135–144 PII: S0953-8984(02)29286-3

Domain structure and phase transition in Sc-doped zirconia

G Brunauer[1], H Boysen[1], F Frey[1] and H Ehrenberg[2]

[1] Institute for Crystallography und Applied Mineralogy, LMU München, Theresienstraße 41, D-80333 München, Germany
[2] Institute for Materials Science, TU Darmstadt, Petersenstraße 23, D-64287 Darmstadt, Germany

Received 29 September 2001, in final form 13 November 2001
Published 13 December 2001
Online at stacks.iop.org/JPhysCM/14/135

Abstract

The temperature dependence of the domain structure associated with the ferroelastic phase transition ($Fm\bar{3}m \leftrightarrow R\bar{3}m$) in ZrO_2 doped with 11% Sc_2O_3 has been determined from a peak shape analysis of high-resolution synchrotron x-ray powder diffraction data. In the temperature region of coexisting phases the observed characteristic anisotropic broadening and asymmetry of the lines is modelled by three different phases: a main rhombohedral phase, a distorted rhombohedral phase with a smaller c/a ratio, and a cubic phase. The latter two are assigned to the internal structure of the domain walls between two adjacent twin domains. The size and amount of the cubic phase show an initially slow increase with temperature followed by a very steep increase and a slow one after that. The size of the (main) rhombohedral domains remains nearly constant, while (micro-) strain in the distorted regions gradually decreases.

(Some figures in this article are in colour only in the electronic version)

1. Introduction

Scandium-doped zirconia $x Sc_2O_3 \cdot (1 - x) ZrO_2$ (ScZ) is known for its excellent oxygen ionic conductivity at high temperatures and is therefore a promising candidate for technical application, e.g., in fuel cells. A drawback is, however, the aging effect, i.e. the reduction of the ionic conductivity with operating time, which is not yet fully understood. Depending on the doping content x, temperature, and aging time, different structures and phase compositions occur. In particular, samples with high conductivity, i.e. those with $x = 9$, 10, and 11 mol% Sc_2O_3 (S9, S10, S11 in the following) have been investigated previously by means of neutron and x-ray diffraction at room temperature and at 1000 °C (the usual operating temperature) both before and after aging (1000 h at 1000 °C) [1]. The starting materials of S9, S10, and S11 are tetragonal (**T**, space group $P4_2/nmc$) + cubic (**K**, space group $Fm\bar{3}m$), cubic (**K**), and rhombohedral (**R**′, space group $R\bar{3}$), respectively. The structure of **R**′ has a very large supercell and has not yet been solved completely. After aging, S9, S10, and S11 become

T + **K** with a different phase ratio, **K** + **R**′, and **R**′, respectively. This is in agreement with the fact that S10 shows the highest ionic conductivity, while the larger amount of possible oxygen vacancies in S11 tend to order, thus becoming unavailable for the conduction process. A partial ordering has taken place during the aging of S10 as evidenced by the small amount of **R**′ phase (about 10%) which can explain the aging effect. At high temperatures (1000 °C) in all cases the fluorite structure (space group $Fm\bar{3}m$, with disordered cations and vacancies on the anion sites) appears. The previous neutron scattering experiments gave hints of an anisotropic broadening of the peaks [1]. This was reminiscent of results found earlier at the ferroelastic phase transition in $PbTiO_3$, which was interpreted in terms of a specific domain structure within the powder grains [2]. Therefore high-resolution synchrotron experiments were performed on a non-aged 11% Sc_2O_3-doped sample as a function of temperature.

2. Experiment

The experiments were performed in Debye–Scherrer mode at the high-resolution powder diffractometer at beamline B2 of the HASYLAB Hamburg with a Ge(111) analysing crystal between sample and detector. The samples were held in quartz capillaries and were diluted with 80% diamond powder in order to reduce absorption. Monochromatic photons were selected from the white beam of a bending magnet by a Ge(111) double-crystal monochromator, and the wavelength was refined to 1.1783 Å, based on the reflection positions of a Si-NBS(640b) standard. The STOE furnace used was stable within 0.2 °C, and the absolute temperature was calibrated before the experiment with an accuracy of about 5 °C. Full patterns were measured at room temperature, 300, 500, and 600 °C. In addition, intensity data were recorded for only two reflection sets ($(111)_{\mathbf{K}} \rightarrow (003)_{\mathbf{R}}$, $(101)_{\mathbf{R}}$ and $(220)_{\mathbf{K}} \rightarrow (104)_{\mathbf{R}}$, $(110)_{\mathbf{R}}$) at intermediate temperatures to allow for an analysis of the temperature dependence of profiles and a refinement of lattice parameters. Reflection profiles were fitted by pseudo-Voigt functions in the formulation of Thomson *et al* [3], which allows refinement of both Gaussian and Lorentzian size and strain parameters, using the Rietveld refinement program FULLPROF [4].

Here the full width at half-maximum is calculated from

$$\begin{aligned} \mathrm{fwhm}_G^2 &= (U_i + U_G^2)\tan^2\Theta + V_i\tan\Theta + W_i + Y_G/\cos^2\Theta \\ \mathrm{fwhm}_L &= U_L\tan\Theta + (Y_i + Y_L)/\cos\Theta \end{aligned} \tag{1}$$

where U_i, V_i, W_i, and Y_i are taken to describe the instrumental resolution, and U_G/U_L and Y_G/Y_L are the isotropic Gaussian and Lorentzian strain and size parameters, respectively, from which the strains (in %) and sizes (in Å) are derived, and

$$\begin{aligned} \varepsilon_G &= (\pi/1.8)\sqrt{U_G^2} \qquad & \varepsilon_L &= (\pi/1.8)U_L \\ L_G &= (180/\pi)\lambda/\sqrt{Y_G} \qquad & L_L &= (180/\pi)\lambda/Y_L. \end{aligned} \tag{2}$$

3. Results

At room temperature the rhombohedral structure **R**′ with $a_{\mathbf{R}'} \approx \sqrt{31}a_{\mathbf{R}}$ and $c_{\mathbf{R}'} \approx 2c_{\mathbf{R}}$ is observed. Although a good data set is available, a determination of the structure with this very large supercell has not been successful up to now. With increasing temperature the corresponding superlattice peaks gradually disappear. At 500 °C a simple rhombohedral cell derived from the cubic cell with lattice constant $a_{\mathbf{K}}$ through $a_{\mathbf{R}} \approx a_{\mathbf{K}}/\sqrt{2}$, $c_{\mathbf{R}} \approx a_{\mathbf{K}}\sqrt{3}$ (**R**, $R\bar{3}m$) is reached. Between 500 and 600 °C this phase coexists with the high-temperature cubic phase (**K**). Above 600 °C only the latter is present. The **K** ↔ **R** transition is ferroelastic and of first order as evidenced by the coexistence of the two phases in this temperature range.

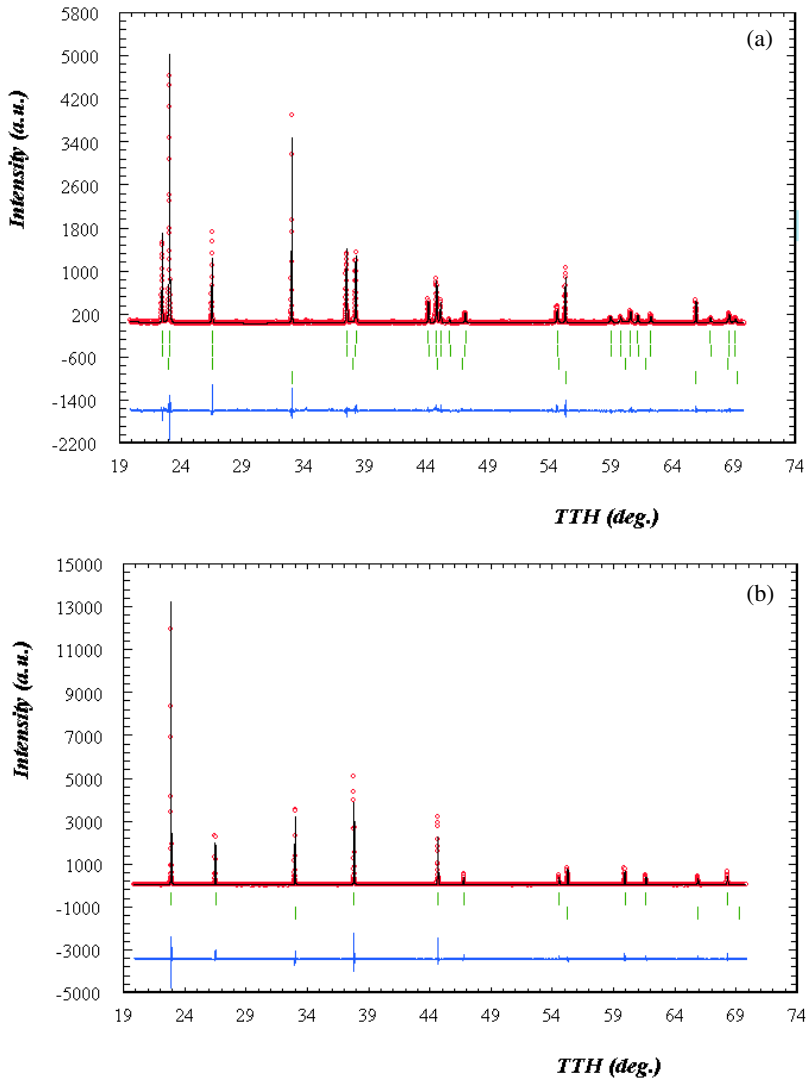

Figure 1. Observed and calculated powder diagrams of $Sc_{0.22}Zr_{0.78}O_{1.89}$ at 500 °C (a) and 600 °C (b). Tick marks refer to **R**1, **R**2, **K**, diamond (from top, (a)) and **K**, diamond (b), respectively.

Figure 1 shows full patterns taken at 500 and 600 °C, while in figure 2 examples of the temperature evolution of a selected reflection group are displayed. Apparently, reflections which are split in the **R** phase show characteristic broadening and asymmetry with tails in the direction of the corresponding cubic reflections (figure 3(a)), while those which do not split stay relatively sharp (figure 3(b)). The diamond lines are generally much sharper than the ScZ ones and are therefore taken to describe the instrumental resolution, i.e. the refined values of U_i, V_i, W_i and Y_i in equation (1) for this phase were used as standard values and kept fixed also for ScZ. To describe the additional broadening of S11, only the parameters U_G, U_L, Y_G, and Y_L were allowed to vary. The cubic reflections are very weak and broad at the beginning and become sharper and stronger with increasing temperature. In order to model the asymmetry, as

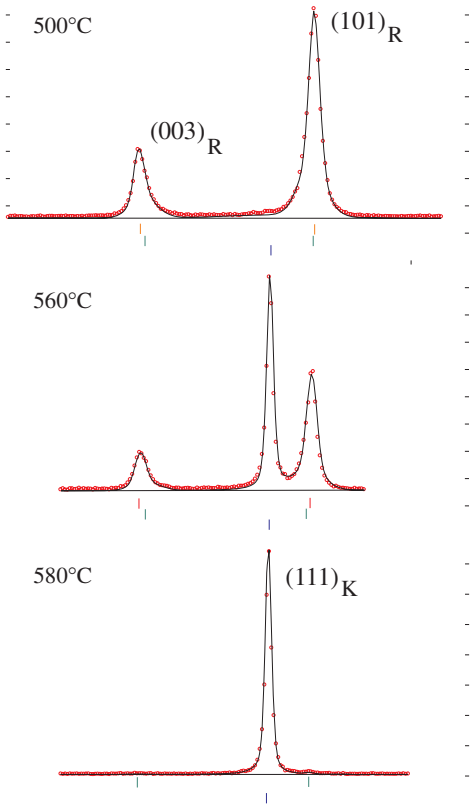

Figure 2. Observed (circles) and calculated (with domain model, straight line) intensities of $Sc_{0.22}Zr_{0.78}O_{1.89}$ at 500, 560, and 580 °C (from top).

a first approximation, two rhombohedral phases **R1** and **R2** with identical structures but with different c/a ratios were introduced in addition to the cubic phase **K**. As can be seen in figures 1 and 2, satisfactory fits can be obtained in this way, although they are not perfect (see below). At 580 °C the rhombohedral lines become too weak and only one (average) rhombohedral phase could be fitted reliably. In addition to the ratios of the amounts of the three phases, different models have been tried to describe the different linewidths of the three phases. Various test refinements showed that not all possible parameters in (1) can be refined independently and that best results are obtained by allowing only Y_L for the main rhombohedral and the cubic phases and ε_G for the second rhombohedral phase as additional parameters to describe the size and strain broadening. The results are summarized in figures 4 (lattice constants), 5 (c/a ratio), 6 (amount of phase), 7 (size), 8 (strain), and 9 atomic displacement parameters (ADPs).

4. Discussion

The results can be interpreted in terms of the appearance of twin domains arising from the symmetry loss at the phase transition which corresponds to the ferroelastic Aizu species $m3mF\bar{3}m$ [5]. This leads to four different orientations of the domains with nine allowed wall orientations between them (W-walls corresponding to {100} and {110} plane families) [6]. These walls are not infinitely thin, but include a gradual change from one orientational state

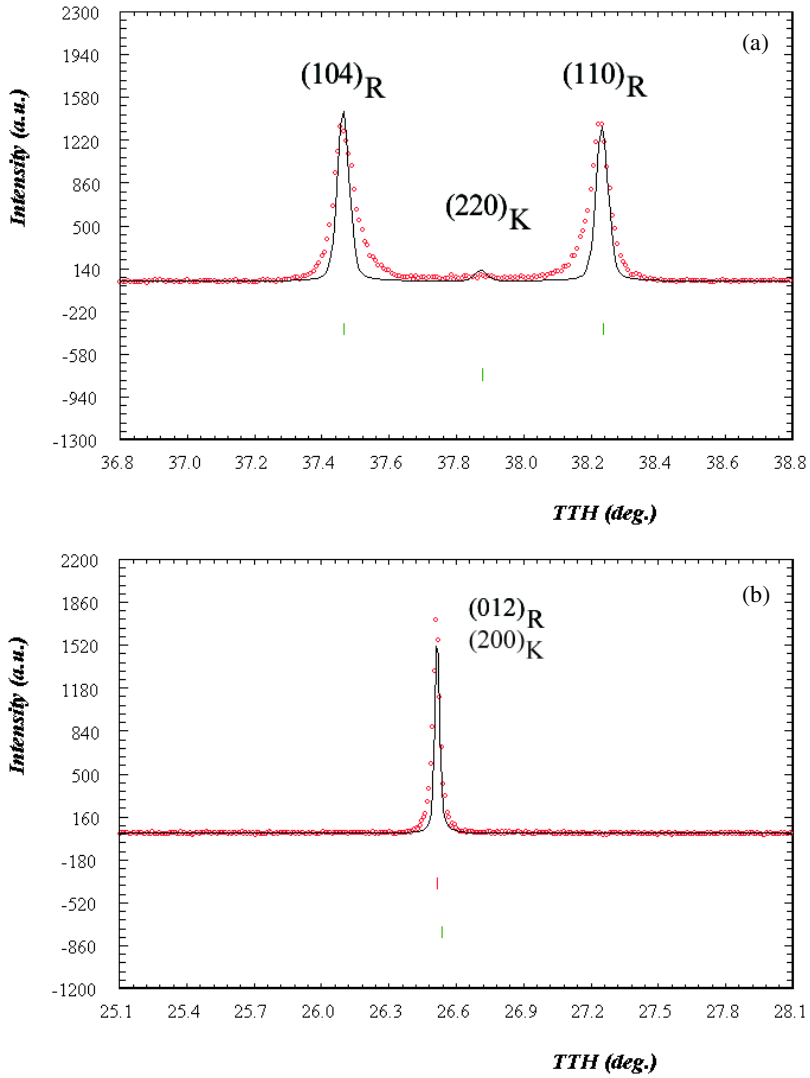

Figure 3. (a) Observed (circles) and calculated (with instrumental resolution only, solid curve) intensities of $Sc_{0.22}Zr_{0.78}O_{1.89}$ at 500 °C. (b) Observed (circles) and calculated (with instrumental resolution only, solid curve) intensities of $Sc_{0.22}Zr_{0.78}O_{1.89}$ at 500 °C.

to the other, thereby passing through a region with the symmetry of the parent structure, as illustrated schematically in figure 10. Here, as an approximation, the intermediate region between the adjacent domains has been divided into a distorted 'rhombohedral' and a 'cubic' one. According to this model, the phases used in the fits can be assigned to: **R1**, the main rhombohedral phase; **R2**, the distorted rhombohedral regions, with a smaller c/a ratio; and **K**, the cubic region. Note that such a model is in agreement with the findings during the trial fits: **R1** and **K** can be described in terms of their particle sizes, while the heavily distorted **R2** is dominated by the strain.

The lattice constants (figure 4) show a normal general increase with temperature. The average pseudocubic values of both **R1** and **R2**, defined as $a_k(\mathrm{av}) = (a^2c\ 2/\sqrt{3})^{1/3}$, coincide

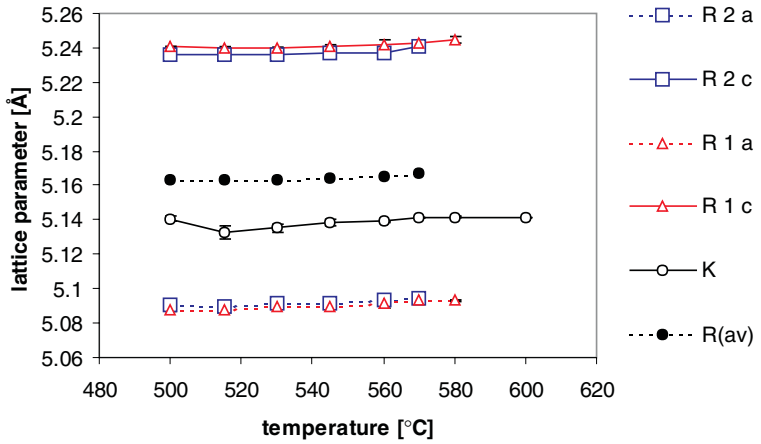

Figure 4. Temperature variations of lattice constants. For comparison, the pseudocubic values $a_{\mathbf{K}}^{pc-a} = a_{\mathbf{R}}\sqrt{2}$ and $a_{\mathbf{K}}^{pc-c} = c_{\mathbf{R}}/\sqrt{3}$ are shown for the rhombohedral phases.

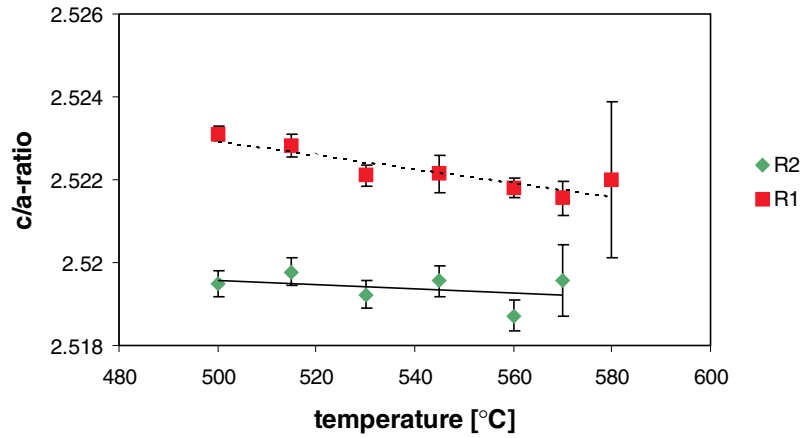

Figure 5. Temperature variations of the c/a ratios.

perfectly with each other (therefore, only one is shown in figure 4), whereas the actual values of **K** are slightly lower, indicating a small volume anomaly at the transition. The c/a ratios (figure 5) decrease only slightly with temperature, i.e. there is a strong jump-like behaviour in agreement with the first-order character of the transition. Up to 545 °C the cubic content (figure 6) is manifested only by rather weak and broad maxima corresponding to a phase content of 5–10%. Around 560 °C, this amount increases rapidly up to about 50% and forms sharp reflections. The amount of the distorted phase **R2** initially increases slightly at the costs of **R1**. At 600 °C all **R** phases have disappeared. The size of **R1** (figure 7) stays relatively constant over the whole temperature region at about 560 Å, while that of **K** increases from about 280 Å through 730 Å towards about 1200 Å at high temperatures. The strains in **R2** (figure 8) decrease with temperature which may be understood in view of the concomitant decrease of the c/a ratio. Figure 9 shows the temperature dependence of the atomic displacement parameters of oxygen. Due to the limited information from only two sets of reflections for most temperatures, those of Zr/Sc have been constrained to the ratios $B_{\mathrm{Zr/Sc}}/B_{\mathrm{O}}$ found from the full patterns at 500 and 600 °C, respectively. As can be seen, they increase and decrease dramatically for

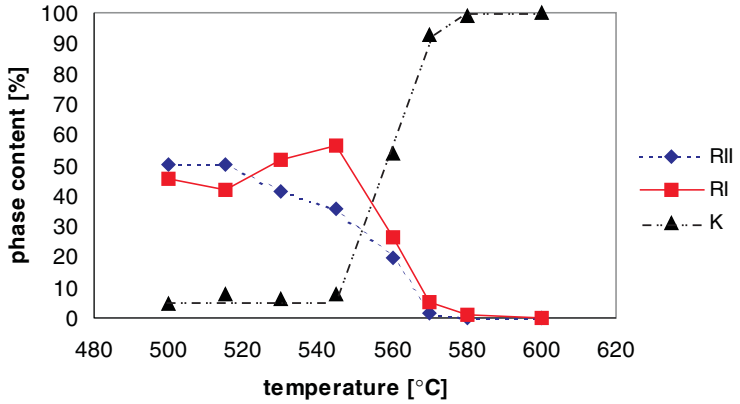

Figure 6. Temperature variations of the phase contents.

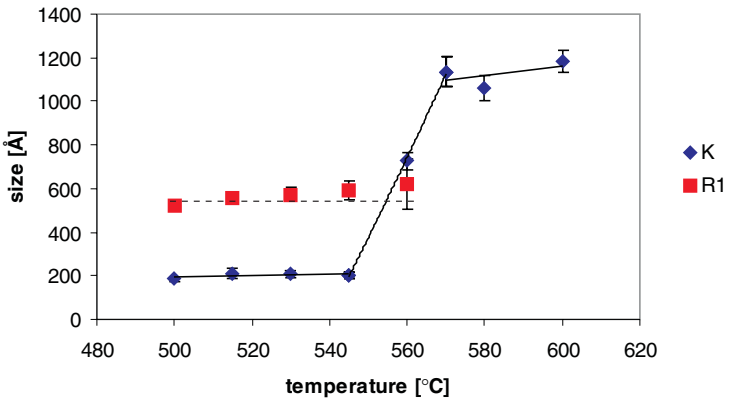

Figure 7. Temperature variations of domain sizes.

the **R** and **K** phase, respectively. This is another indication of the inherent disorder when the respective phase is present only in small amounts.

Although final results should take into account more accurately the gradual variation of the c/a ratio in the distorted regions of the domain wall, the main characteristics of the evolution of the domain structure at this ferroelastic phase transition become clear within the approximations used. Initially large domains (twins) of the main low-temperature phase **R1** exist, with walls between them consisting of both a distorted region **R2** and a proper cubic region **K**. Note that the cubic phase exhibits separated peaks, i.e. there is not a continuous change from one orientational state to the other, but a clearly separated region with the structure of the high-temperature phase. These cubic nuclei increase relatively suddenly in size, whereas the size of the rhombohedral regions remains relatively unaffected up to the final disappearance of all remaining rhombohedral phases. While the fits for the splitting reflections are relatively good (figure 2), there are still discrepancies for those that do not split (figure 11): the calculated lines are broader than the observed ones. There are two possible explanations:

(i) For simplicity we have used isotropic strain and particle broadening parameters, whereas they should in fact be anisotropic, since the domain walls are planar. Unfortunately, the limited number of reflections which could be measured in the present experiment did not allow for a refinement of anisotropic strain broadening.

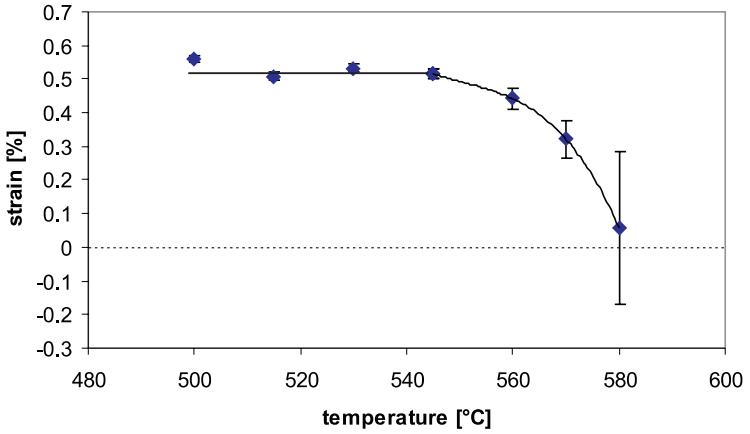

Figure 8. The strain effect of the *R*2 phase.

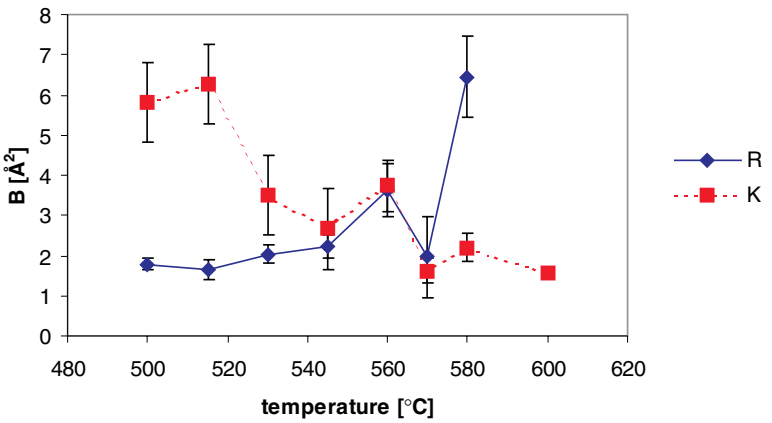

Figure 9. ADPs of the rhombohedral and cubic phases.

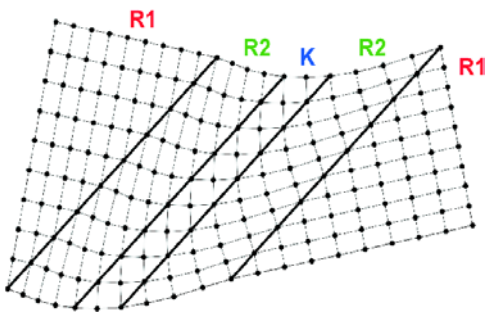

Figure 10. A schematic model of the domain walls.

(ii) There should be at least some coherence between adjacent domains. This invalidates the superposition of the intensities of the different phases as used here, i.e. a more sophisticated model should include the superposition of the scattering amplitudes.

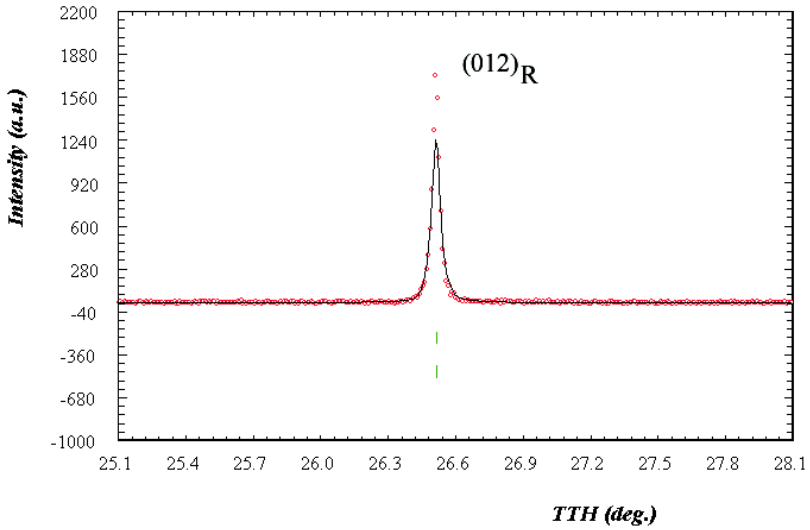

Figure 11. Observed (circles) and calculated (with domain model, solid curve) intensities of the non-splitting reflection $(012)_{\mathbf{R}} = (200)_{\mathbf{K}}$ of $Sc_{0.22}Zr_{0.78}O_{1.89}$ at 500 °C.

5. Conclusions

In spite of some approximations made to describe the characteristic anisotropic and asymmetric line broadening in powder diagrams following the ferroelastic phase transition in ScZ, the basic features of the underlying model should be correct. In its simplest form, at low temperatures each crystallite (which may or may not coincide with a powder grain) consists of several orientational domains (twins) of the low-temperature phase separated by domain walls which include both a heavily strained region and a region of the high-temperature phase. The absolute values of the refined parameters should not be taken too literally, because of the various approximations. In particular, we have no direct estimate of the size of the strained region **R2**, but, since its phase content is roughly the same as that of the proper one **R1**, the size should also be roughly the same.

As mentioned above, at the beginning of the transformation only small amounts of **K** phase are present, but these appear as separated regions as evidenced by the peak-like character of the corresponding reflections (figure 2). This rather surprising fact is at variance with the usually expected hyperbolic tangent behaviour of the order parameters across the domain wall [7]. From the present evidence we cannot exclude the possibility that these peaks may in fact be due to some very small particles within the powder sample (for which a lowering of the transition temperature has been observed in other cases, e.g. for $BaTiO_3$ [8, 9]) or due to a relaxation at the surface of the particles.

In any case, the existence of domains within the crystallites can be safely concluded from the fact that the calculated widths of the reflections that do not split are larger than the observed ones. Otherwise, i.e. if the broadening were simply due to different crystallite sizes within the sample, this would lead to a broadening of these reflections too. In other words, planar defects (the walls) and, probably, coherence effects must be present.

It should be emphasized that the results found here are characteristic of powder samples consisting of small crystallites, while in single crystal, domains with sizes larger than the dimensions of the crystallites may exist (e.g. $PbTiO_3$; see [10]).

In conclusion, a discussion of ferroelastic phase transitions in powders in terms of Landau theory must include the spatial variation of the order parameter. This effect was discussed in some detail by Salje and co-workers for clamped particles [11] and the effect of strains [12,13].

Acknowledgments

This work was supported by the DFG under Bo1199/1-2. We would also like to thank E Salje for very helpful discussion of the strain effects at ferroelastic phase transitions.

References

[1] Göbel U, Boysen H, Lehnert H, Frey F, Hohlwein D and Schneider R 2000 *Z. Kristallogr.* S **17** 212 (abstract)
Göbel U 1999 *Diplomarbeit* LMU München
[2] Lehnert H, Boysen H, Schneider J, Frey F, Ehrenberg H and Radaelli P 2000 *Z. Kristallogr.* S **17** 216
Lehnert H, Boysen H, Schneider J, Frey F, Ehrenberg H and Radaelli P 2002 in preparation
[3] Thompson P, Cox D E and Hastings J B 1987 *J. Appl. Crystallogr.* **20** 79
[4] Rodriguez-Carvajal J and Roisnel T *Laboratoire Leon Brillouin (CEA-CNRS) (Saclay, France)*
[5] Aizu K 1970 *J. Phys. Soc. Japan* **28** 706
[6] Sapriel J 1975 *Phys. Rev.* B **12** 5128
[7] Salje E K H 1990 *Phase Transition in Ferroelastic and Co-elastic Crystals Student Edition* (Cambridge: Cambridge University Press)
[8] Gläsel H-J, Hartmann E, Hrisch D, Böttcher R, Klimm C, Michel D, Semmelhack H-C, Hormes J and Rumpf H 1999 *J. Mater. Sci.* **34** 2319
[9] Wada S, Suzuki T and Norma T 1995 *Japan. J. Appl. Phys.* **34** 5368
[10] Lehnen P, Dec J and Kleemann W 2000 *J. Phys. D: Appl. Phys.* **33** 1932
[11] Pertsev N A and Salje E K H 2000 *Phys. Rev.* B **61** 902
[12] Bratkovsky A M, Salje E K H, Marais S C and Heine V 1995 *Phase Transitions* **55** 79
[13] Bratkovsky A M, Heine V and Salje E K H 1996 *Phil. Trans. R. Soc.* A **354** 2875